Available online at www.sciencedirect.com
ScienceDirect
ELSEVIER
ISPRS Journal of Photogrammetry & Remote Sensing xx (2007) xxx – xxx
PHOTOGRAMMETRY & REMOTE SENSING
www.elsevier.com/locate/isprsjprs

Testing satellite and ground thermal imaging of low-temperature fumarolic fields: The dormant Nisyros Volcano (Greece)

E. Lagios [a,*], S. Vassilopoulou [a], V. Sakkas [a], V. Dietrich [b], B.N. Damiata [c], A. Ganas [d]

[a] *Space Applications Research Unit in Geosciences, Laboratory of Geophysics, Department of Geophysics & Geothermics, University of Athens, Panepistimiopolis-Ilissia, 157 84 Athens, Greece*
[b] *Swiss Federal Institute of Technology, Institute of Mineralogy and Petrography, ETH-Zentrum, CH-8092 Zurich, Switzerland*
[c] *Cotsen Institute of Archaeology, University of California, Los Angeles, CA, USA*
[d] *National Observatory of Athens, Geodynamic Institute, P.O. Box 20048, 118 10 Athens, Greece*

Received 7 June 2005; received in revised form 13 July 2007; accepted 16 July 2007

Abstract

The Nisyros Volcano (Greece) was monitored by satellite and ground thermal imaging during the period 2000–2002. Three night-scheduled Landsat-7 ETM$^+$ thermal (band 6) images of Nisyros Island were processed to obtain land surface temperature. Ground temperature data were also collected during one of the satellite overpasses. Processed results involving orthorectification and 3-D atmospheric correction clearly show the existence of a thermal anomaly inside the Nisyros Caldera. This anomaly is associated mainly with the largest hydrothermal craters and has land surface temperatures 5–10 °C warmer than its surroundings. The ground temperature generally increased by about 4 °C inside the main crater over the period 2000–2002. Ground thermal images of the hydrothermal Stephanos Crater were also collected in 2002 using a portable thermal infrared camera. These images were calibrated to ground temperature data and orthorectified. A difference of about 0–2 °C was observed between the ground thermal images and the ground temperature data. The overall study demonstrates that satellite remote sensing of low-temperature fumarolic fields within calderas can provide a reliable long-term monitoring tool of dormant volcanoes that have the potential to reactivate. Similarly, a portable thermo-imager can easily be deployed for real-time monitoring using telemetric data transfer. The operational costs for both systems are relatively low for an early warning system.

Keywords: Nisyros Volcano; Satellite Remote Sensing; Landsat ETM$^+$; Thermal Infrared Camera; Early Warning System

1. Introduction

Quiescent, but active, volcanoes in regions of high geodynamic unrest potentially represent a severe hazard that requires integrated monitoring, satellite surveying and modelling. Remote sensing from satellites has become a powerful tool in monitoring volcanic fields (Todesco et al., 2003; Chen and Zhou, 2004; Patrick et al., 2004), and in particular the use of Landsat Thermal InfraRed (TIR) imagery (e.g. Gaonac'h et al., 1994). For those volcanoes with high surface temperatures above 150 °C, short-wavelength IR (SWIR) bands 5 (1.55–1.175 μm) and 7 (2.08–2.35 μm) of the Landsat Thematic Mapper (TM) have successfully been used (Dozier, 1984; Rothery et al., 1988; Oppenheimer, 1991). Since many

* Corresponding author. Tel.: +30 210 7274424; fax: +30 210 7272787.
E-mail address: lagios@geol.uoa.gr (E. Lagios).

0924-2716/$ - see front matter © 2007 International Society for Photogrammetry and Remote Sensing, Inc. (ISPRS). Published by Elsevier B.V. All rights reserved.
doi:10.1016/j.isprsjprs.2007.07.003

geodynamically active volcanic fields remain under dormant conditions, they exhibit only low-temperature surface conditions below 100 °C and, thus, only can be investigated using band 6 (10.4–12.5 μm) of the Landsat TM or Landsat Enhanced Thematic Mapper (ETM$^+$).

The surface temperature of the Nisyros Volcano has been studied previously using space-based techniques. Earlier work (Ganas and Lagios, 2003) used band 6 of the Landsat TM to map the variation of land surface temperature with topography to an accuracy of 0.4–2 °C. However, the low-temperature (≈ 100 °C) fumarolic activity within the craters could not be detected on bands 5 and 7.

The aim of the present study was the establishment of a low-cost monitoring system of the low enthalpy of the Nisyros Volcano based on satellite (ETM$^+$ band 6) and ground thermal imaging. Since Nisyros has the potential to reactivate, a calibration to baseline conditions is required; if temperature increases are noticed in the future, then increased monitoring and study could be undertaken. A portable TIR camera was used to obtain better spatial resolution of temperatures inside the crater in order to compare them with the satellite-derived and ground-based temperatures (2-D validation). The ground TIR images were calibrated with the temperatures measured in the field and orthorectified prior to comparing them with the satellite data.

2. Volcanic hydrothermal activity

Nisyros Island is a Quaternary volcano located at the easternmost end of the Aegean Volcanic Arc, south of Kos Island in the Dodecanese Archipelago (Fig. 1). Nisyros is a remnant of a prehistoric volcanic field from where the largest known eruption (Kos Plateau Tuff) in the Eastern Mediterranean devastated the entire Dodecanese island chain some 160,000 years ago (GEOWARN, 2003; Volentik et al., 2005; Vanderkluysen et al., 2005). Although the last magmatic activity on the island dates back at least 25,000 years, high seismic unrest, thermal waters and fumarolic gases provide evidence of its continued activity. Violent hydrothermal eruptions accompanied by strong earthquakes occurred in 1871–1873 and 1888 (Gorceix, 1873a,b,c; Gorceix, 1874a,b; Marini et al., 1993) leaving large craters. From 1996 to 1998, the island experienced an episode of geodynamic unrest that included a series of shallow earthquakes up to magnitude M=5.5 (Papadopoulos et al., 1998), a considerable temperature increase in the hydrothermal system (Chiodini et al., 2002), and ground deformation (Lagios et al., 2005).

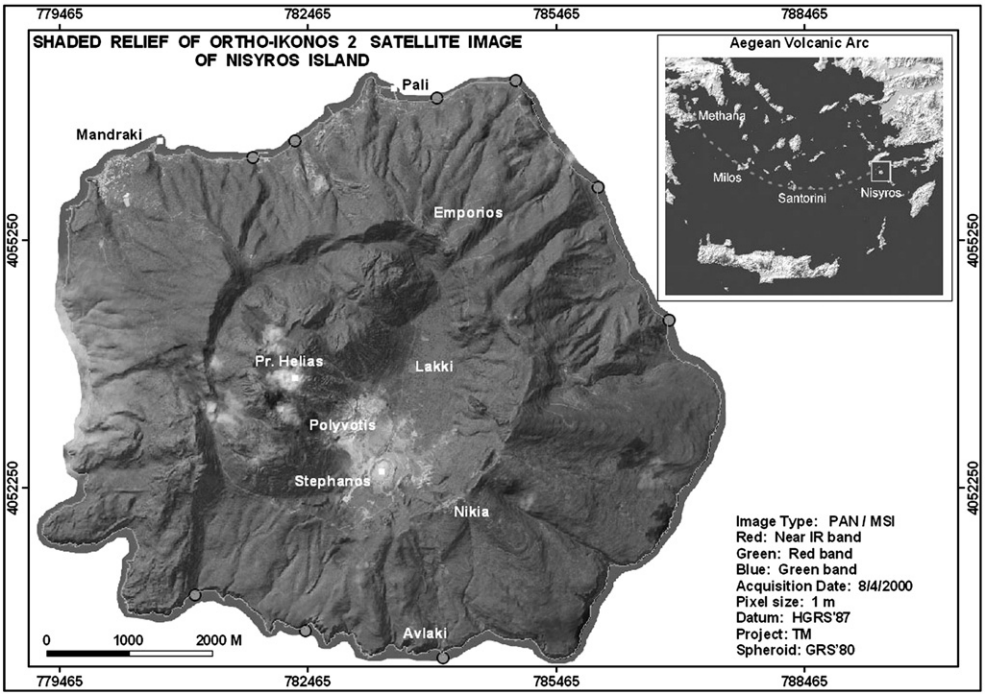

Fig. 1. Orthorectified IKONOS-2 image of Nisyros Island (local datum: HGRS'87) showing the hydrothermal craters (Stephanos and Polyvotis) in the Lakki Plain within the Nisyros Caldera. Circles indicate the location of hot springs at sea level. The insert shows the position of Nisyros Island at the eastern end of the Aegean Volcanic Arc.

Please cite this article as: Lagios, E. et al. Testing satellite and ground thermal imaging of low-temperature fumarolic fields: The dormant Nisyros Volcano (Greece). ISPRS Journal of Photogrammetry & Remote Sensing (2007), doi:10.1016/j.isprsjprs.2007.07.003

The volcanic complex on Nisyros comprises a succession of calc-alkaline lavas and pyroclastic rocks, with a central summit caldera that has an average diameter of 4 km. A large hydrothermal system (Geotermica Italiana, 1983, 1984; Dawes and Lagios, 1991) with brine temperatures above 300 °C at a 1700 m depth is indicated by the existence of numerous, irregularly distributed fumaroles and five larger hydrothermal explosion craters within the caldera. Outside of the caldera, the system includes nine hot springs with temperatures between 30–60 °C that are distributed around the island at sea level (see Fig. 1).

The geochemical model of the hydrothermal system is based on the chemical and the isotopic composition of hydrothermal fluids (fumaroles and thermal springs) and data from two geothermal wells located on the floor of the Lakki plain. These data suggest that the hydrothermal system consists of four main zones (GEOWARN, 2003). The first zone is a magmatic body that supplies heat and fluids to the hydrothermal system. The presence of a degassing magma body is supported by the isotopic compositions of fumarolic H_2O, S and He. The second zone is a deep boiling reservoir with saline brines at temperatures of 300–350 °C. It is fed by a mixture of volcanic and marine sources. The carbon isotopes of CO_2 and CH_4 in fumarolic gases are fixed by isotopic exchange at the temperature conditions of this reservoir. The third zone consists of intermediate reservoirs at variable temperatures, which are fed by the vapour produced by the deeper boiling reservoir. The CO content of the vapour is controlled by the lowest temperatures (generally in the range 180–260 °C) of these intermediate reservoirs. The presence of the intermediate reservoirs is supported by deep drilling data. Finally, several zones of discharge with different kinds of manifestations are present, i.e. soil diffuse degassing structures and fumaroles (located in the Lakki plain), and thermal springs (located along the coastline). A shallow hot aquifer is also present in the area, fed by large quantities of condensates.

3. Data acquisition

The ETM$^+$ band 6 sensor onboard the Landsat-7 satellite measures energy emitted from the Earth's surface (10.4–12.5 μm) at a spatial resolution of 60 m. The repeat cycle of image acquisition is 16 days. These characteristics are suitable for the study of smaller volcanoes and hydrothermal fields with fumaroles and small explosion craters (ranging in diameters between 100–250 m) such as those of the Nisyros Volcano. Night-time imagery was chosen in order to remove the topographic signal evident in the day scenes and to reduce the extent to which daytime solar heating "masks" the volcanogenic heat signal.

The ETM$^+$ Fast-L7A images of October 20, 2000 and October 26, 2002, as well as the ETM$^+$ image of May 19, 2002 were acquired in Level 1G (systematic, GeoTiff format; see Table 1) with radiometric and geometric corrections. A portable TIR camera (NEC Thermo Tracer

Table 1
Acquisitions of Landsat 7 ETM$^+$ night satellite images of Nisyros Island and parameters used for atmospheric correction

Landsat-7 ETM$^+$ acquisitions	Area	Atmospheric model	Parameters of atmospheric model (in altitude: 0–1 km)	RMS ([a])(°C)	Local meteorological data
Oct. 20, 2000	Nisyros Island	"1976 US Standard Atmosphere"	Air temperature (T): 15 °C Atm. pressure (P): 1013 mbar Relative humidity (H): 46%	0.5	T: 17 °C P: 1003 mbar H: 49%
	Lakki Plain	"Sub-arctic Summer Atmosphere"	T: 15 °C P: 1010 mbar H: 75%	3.1	Visibility: 20–25km
May 19, 2002	Nisyros Island	"1976 US Standard Atmosphere"	T: 15 °C P: 1013 mbar H: 46%	0.3	T: 15 °C P: 998 mbar H: 33%
	Lakki Plain	"Sub-arctic Summer Atmosphere"	T: 15 °C P: 1010 mbar H: 75%	3.2	Visibility: 20–25 km
Oct. 26, 2002	Nisyros Island	"Mid-latitude Summer Atmosphere"	T: 21 °C P: 1013 mbar H: 76%	0.3	T: 16 °C P: 1015 mbar H: 71%
	Lakki Plain	"Sub-arctic Summer Atmosphere"	T: 15 °C P: 1010 mbar H: 75%	2.9	Visibility: 15–20 km

[a] Root mean square error between field temperature values and calculated (modelled) temperature values.

Please cite this article as: Lagios, E. et al. Testing satellite and ground thermal imaging of low-temperature fumarolic fields: The dormant Nisyros Volcano (Greece). ISPRS Journal of Photogrammetry & Remote Sensing (2007), doi:10.1016/j.isprsjprs.2007.07.003

TH7102 with spectral range from 8–14 μm and 0.08 °C resolution at an error of ± 2%) was also used to acquire ground images at the time of the Landsat-7 overpass in October 2002. The camera was mounted on a stable tripod at a viewing location on the caldera's rim at Nikia Village (Fig. 1). Image acquisitions with the camera were coincident with ground temperature measurements.

Field campaigns were conducted during 2000 and 2002 to collect, twice a day, ground-truth temperature data that were used to calibrate the surface temperatures derived from the satellite and ground camera images. These data (hereafter ground data) were collected at several locations during the satellite overpass: (i) sea-surface temperatures (SST) at Mandraki and Pali were measured before and after the sampling of land surface temperatures, (ii) inside the Lakki Plain (elevation range 85–100 m), (iii) inside the Stephanos Crater (Fig. 2) and (iv) in the center and close to the coastline of the island. The field measurements were made with a digital thermometer (FLUKE™, thermocouple 80PK-5A, www.fluke.com) with piercing probes that had been calibrated to an accuracy of ± 0.3 °C. The sampling points were established during the first campaign and were reoccupied during the following campaigns.

To assist with geometric correction of both sets of thermal images, a number of ground control points (GCPs) were selected inside and outside the Stephanos Crater that could be easily recognized on the images. Geodetic GPS receivers were used to determine the coordinates of the GCP points. The temperature inside the Stephanos Crater was measured along specific profiles at a 5 m interval, yielding more than 150 ground temperature control points (GTCPs) in and around the crater, aiming to constrain the analysis of the ground TIR images.

4. Landsat image processing

The low-gain thermal band was used for all the images, which were sub-setted to include only the immediate vicinity of Nisyros Island. The Landsat-7 image processing included two steps, an orthorectification and an atmospheric correction. Orthorectification was performed using Geomatica OrthoEngine Basics (2001) software and a digital elevation model with a cell size of 2 m (Vassilopoulou and Hurni, 2001; Vassilopoulou et al., 2002). It was found that the rms errors between the three orthorectified images were less than 1 pixel (60 m × 60 m).

The significant issue of correcting the TIR images (both ground and Landsat-7) for atmospheric effects using ground meteorological data was seriously considered. The ideal approach would be to construct an atmospheric model using radiosonde data. The model could then be applied above the study area at the same time as the TIR imagery acquisition. The radiosonde method, however, was not selected because of budget constraints. Instead, ground meteorological data collected from a nearby (very close to the Stephanos Crater) continuously recording meteorological station was used, registering atmospheric pressure, air temperature and relative humidity.

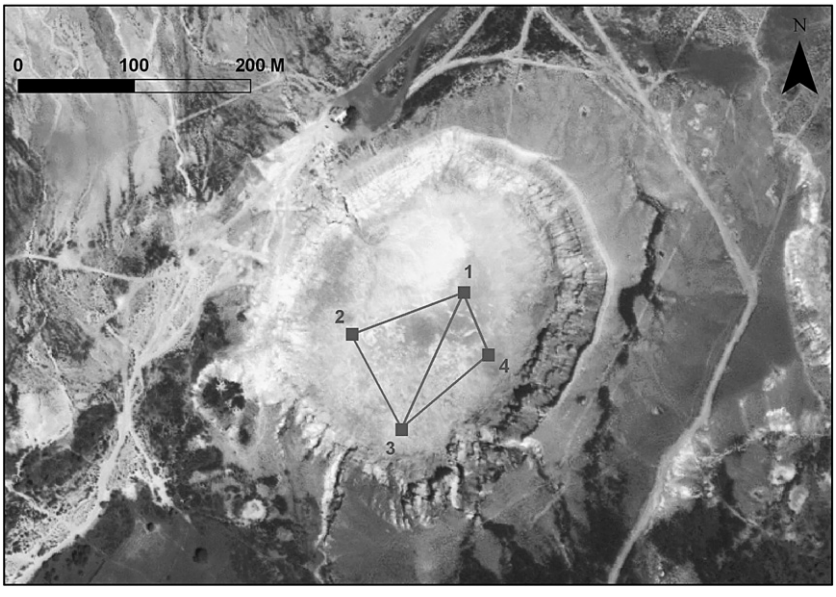

Fig. 2. Orthorectified IKONOS-2 image showing the five profiles inside Stephanos Crater, where ground temperature measurements were collected (5 m interval).

Please cite this article as: Lagios, E. et al. Testing satellite and ground thermal imaging of low-temperature fumarolic fields: The dormant Nisyros Volcano (Greece). ISPRS Journal of Photogrammetry & Remote Sensing (2007), doi:10.1016/j.isprsjprs.2007.07.003

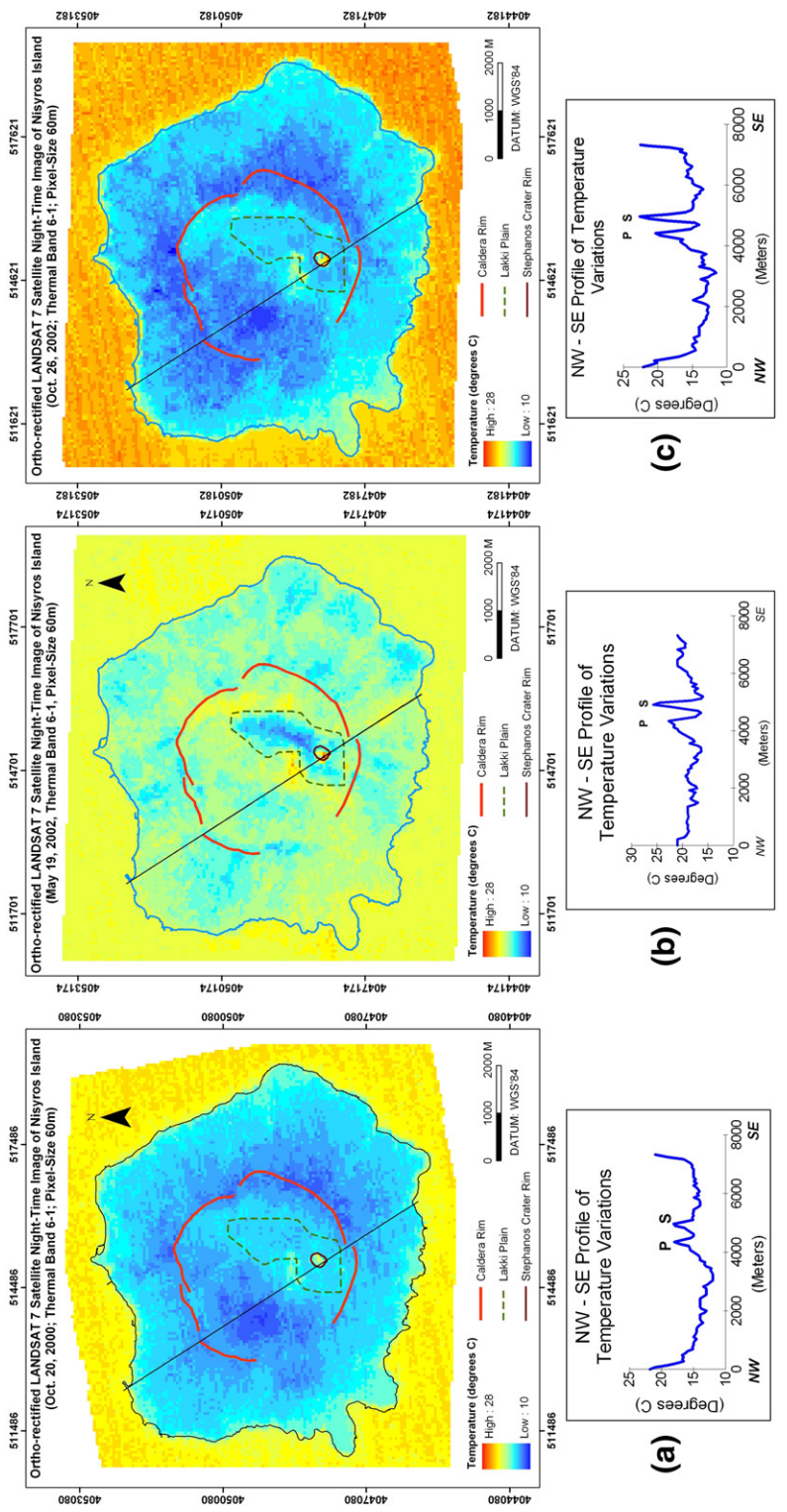

Fig. 3. Orthorectified Landsat-7 ETM^{+} night-time images (a: Oct. 20, 2000; b: May 19, 2002 and c: Oct. 26, 2002) of Nisyros Island. The two areas of higher temperature at Polyvotis (P) and Stephanos (S) craters are shown in the NW–SE temperature profiles (lower diagrams).

Please cite this article as: Lagios, E. et al. Testing satellite and ground thermal imaging of low-temperature fumarolic fields: The dormant Nisyros Volcano (Greece). ISPRS Journal of Photogrammetry & Remote Sensing (2007), doi:10.1016/j.isprsjprs.2007.07.003

The ATCOR3 module of the ATCOR for ERDAS Imagine software (ATCOR, 2002) that performs radiometric correction of satellite imagery over rugged terrain and removes atmospheric and topographic effects was applied for the atmospheric correction. Atmospheric models inherent in the software with fixed values for atmospheric pressure (P), air temperature (T) and relative humidity (H) were selected based on the local meteorological data, including the observed SST during the night of the satellite overpass. The models with the smaller rms error and values of P, T and H that were closer to the ground data were finally adopted (see Table 1). However, it can be seen that the Lakki Plain was treated separately, since this particular area yielded smaller rms temperature errors when analyzed alone, as compared to when grouped with observations from the rest of the island.

The selection of an appropriate ground-surface emissivity (ε) was an issue of concern. Ground-based measurements involving the combination of thermocouple data and the analysis of ground TIR imaging could help to determine realistic emissivity values of the various geological formations of the island. However, since the applied methodology of the present study is based on detecting relative temporal variations of surface temperature from successive satellite images of various times, the calculation of absolute temperature, as deduced by realistically accurate emissivities, was deemed not critical. Moreover, there was limitation in the applied software (ATCOR3) that did not permit user-defined values of emissivity. Available options included a constant scene emissivity (e.g., 0.98) or a surface cover-dependent emissivity based on a classification with other reflected bands (Salisbury and D' Aria, 1992). The former option was selected and ground-surface emissivity was set to 0.98.

A ground-surface emissivity of 0.98 was therefore assumed for all scenes. We note that this value is representative of lavas and pyroclastic rocks in general (Wan et al., 1994; Higgins and Harris, 1997). A 2.5% error in emissivity would yield a 1 °C error in surface temperature (ATCOR, 2002), while an error of less than 5% inside of the Stephanos Crater would yield a 2 °C error, which is close to the error estimation of the land surface temperature, as will be shown below. However, if the surface temperature is about 20 °C higher than the air temperature, as actually is the case inside the Stephanos Crater, the influence of a 2.5% error in emissivity yields an error in surface temperature estimation of about only 1.2 °C. Thus, assuming an emissivity of 0.98 for the whole island, it corresponds to an error of 0.2–1.2 °C for mid-latitude summer conditions, when the single-channel method is applied to determine land surface temperature (Schädlich et al., 2001; Dash et al., 2002).

The Stephanos Crater was also studied using the ground thermal camera. The value of ground-surface emissivity was adjusted as described in Section 5. Based on the above considerations, orthorectified and atmospherically corrected satellite TIR images were produced. These images were imported into ArcGIS software (ESRI, 2001) and land surface temperature maps were produced (Figs. 3 and 4).

Generally, the differences in land surface temperature between the ETM$^+$ values and the observed ground data were similar for all three satellite images. Specifically, the temperature differences (i) of the SST values were

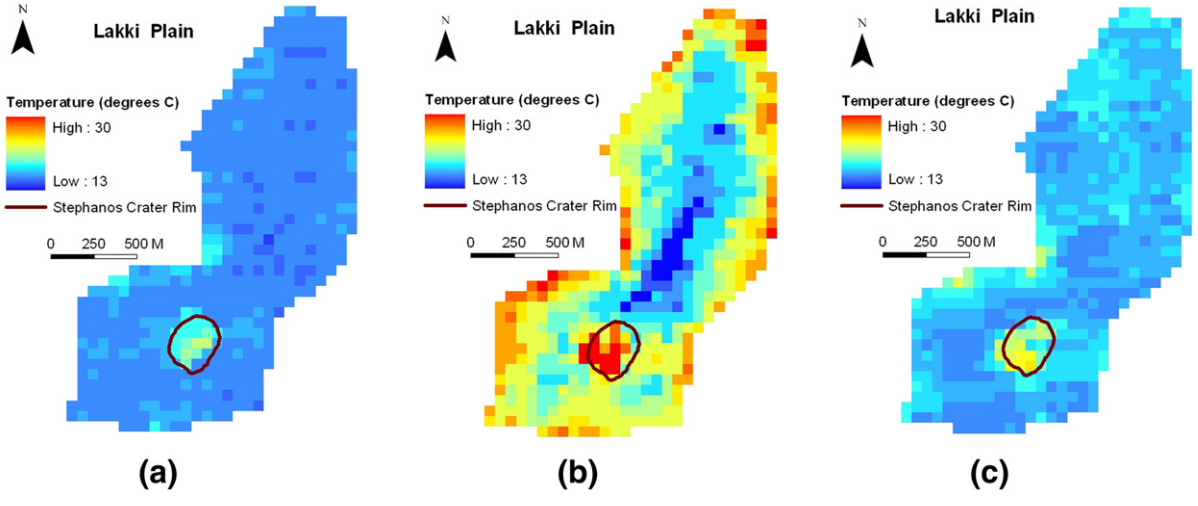

Fig. 4. Enlarged section of the Lakki Plain (Fig. 3) showing the temperature variation of the three Landsat images.

Please cite this article as: Lagios, E. et al. Testing satellite and ground thermal imaging of low-temperature fumarolic fields: The dormant Nisyros Volcano (Greece). ISPRS Journal of Photogrammetry & Remote Sensing (2007), doi:10.1016/j.isprsjprs.2007.07.003

less than 0.5 °C, (ii) inside the Lakki Plain ranged from 1–2 °C, (iii) inside the Stephanos Crater were between 2–3 °C, while for certain pixels were as high as 6 °C, and (iv) close to the coastline and near the center of the island were less than 1 °C. The largest deviations are noticed inside the Lakki Plain and the Stephanos Crater's floor. These temperature differences are attributed to a combination of two effects: (i) the smoothing of the ETM$^+$ pixels (Becker and Li, 1995; Painter et al., 2003) and (ii) a lower ground-surface emissivity, especially in and around the Stephanos Crater, than the 0.98 assumed for processing. For the area close to the coastline, as well as the central portion of the island, the observed temperature differences are comparable to the noise level of the ETM$^+$ sensor (Ganas and Lagios, 2003).

In general terms, the Landsat ETM$^+$ image of May 19, 2002 is warmer than the other two images. However, a Land Surface Temperature Difference (LSTD) map between that image and the previous one was not produced, because the time of the observation and the prevailing meteorological conditions were not similar. However, a LSTD map subtracting the October 2000 image from the October 2002 image was produced (Fig. 5). It was found that the average SST difference around the island was about 2±2 °C. The temperature difference (ΔT) associated with the inland did not change and varied within the error limits: the Lakki Plain, ΔT=1.1±1.2 °C, while for the rest of the island ΔT=0.3±1.0 °C. Only in the Stephanos Crater did the temperature increase, that is ΔT=4.3±1.9 °C. The two pixels showing negative values (− 3 °C and − 4 °C) occurred in the central-eastern part of the crater's floor and is attributed to the watery environment of mud pools that formed in October 2002. Note that the overall areal extent and temperature of the fumaroles within the crater did not change during the period of the observations (GEOWARN, 2003).

5. Ground-based TIR camera imaging

The goal of the detailed ground temperature survey was to produce orthorectified and calibrated ground TIR images for the testing and refinement of the satellite TIR images. To a certain extent, this procedure provided a 2-D surface temperature validation for the processed satellite images. Raw ground-based TIR camera images (hereafter ground TIR images) of the Stephanos Crater (altitude 85 m) were taken from a permanent location at Nikia (altitude 430 m) during the fieldwork campaign in October 2002 (Fig. 6). The camera was positioned overlooking crater, with a western down-looking viewing

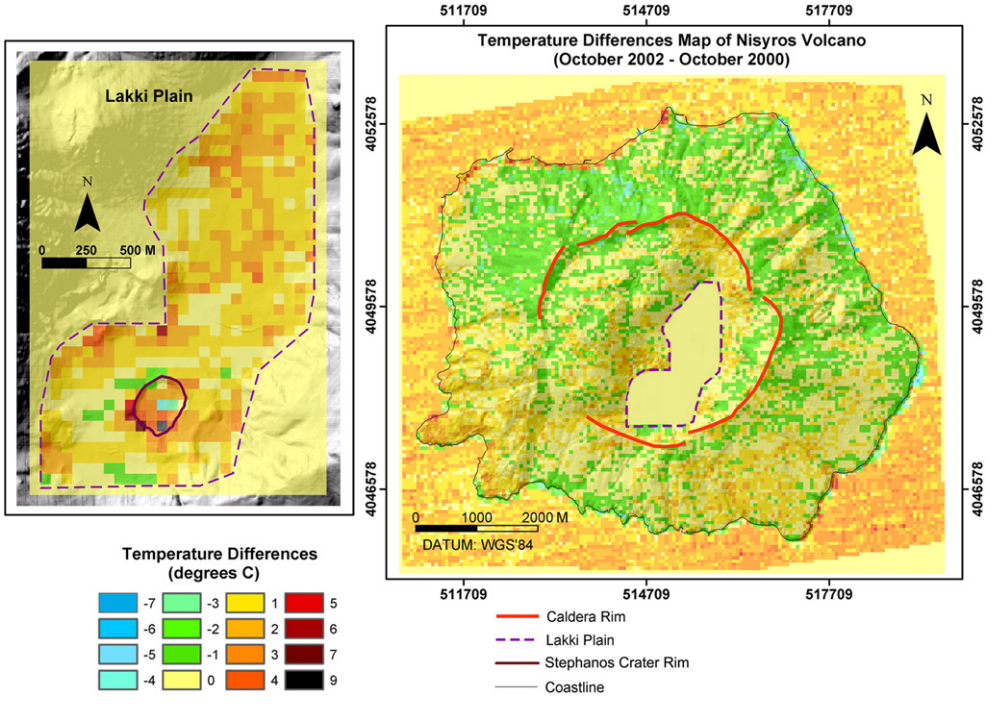

Fig. 5. Land Surface Temperature Difference map of Landsat-7 ETM$^+$ images (Oct. 26, 2002 and Oct. 20, 2000) of Nisyros Island. Enlarged section of the Lakki Plain (left image) indicated as masked area in the right image.

Please cite this article as: Lagios, E. et al. Testing satellite and ground thermal imaging of low-temperature fumarolic fields: The dormant Nisyros Volcano (Greece). ISPRS Journal of Photogrammetry & Remote Sensing (2007), doi:10.1016/j.isprsjprs.2007.07.003

angle of 15° from the horizontal level and at an azimuth of 295° N. At this location, the size of the crater (about 200 m diameter) is about five times smaller than the distance between the crater and the camera location. We noted that small areas of the floor and flank at the eastern part of the crater were obscured from the camera's location and, consequently, the surface temperature at those areas could not be imaged. All other areas are expected to be similarly affected by the atmosphere, independent of their location in the crater. A series of calibrated ground TIR images were produced, after being processed using the IRIS (2001) software, and were then orthorectified applying the selected GCPs. These orthorectified images, however, have a slight eastward shift of less than one pixel (5 m × 5 m) due to the oblique viewing angle.

The Stephanos Crater has heterogeneous geology (i.e., volcanic sediments, hydrothermal soil and salt deposits) where fumaroles exist and evaporation occurs. In such cases, a ground-surface emissivity of about 0.93 is appropriate (Higgins and Harris, 1997). Thus, emissivity values of 0.93 inside the crater and 0.98 around the crater were adopted in the analysis.

GCPs were collected during fieldwork campaigns and identified in the ortho-IKONOS2 image (pixel size of 1 m) of Nisyros Island used for the orthorectification of the thermal images. Ground TIR images with a pixel size of 5 m were finally produced. Fig. 7a is such an image where the temperature ranges from 17–54 °C and was produced from Fig. 6b applying the IRIS (2001) software.

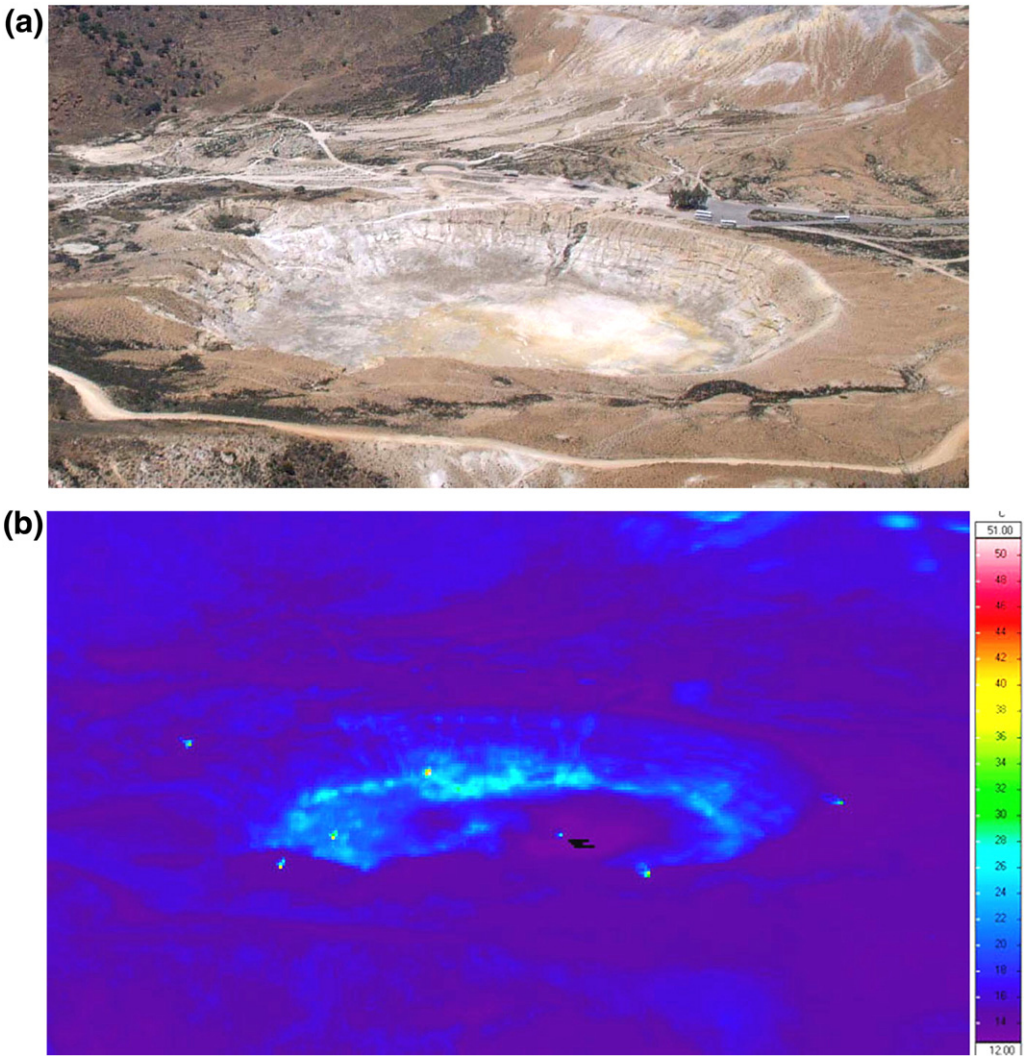

Fig. 6. (a) Outline of the Stephanos Crater viewed from Nikia (400 m elevation, about 300 m above the Lakki Plain, see Fig. 1).(b) Ground-based TIR camera image of the crater viewed from Nikia, showing the surface temperature variations.

Please cite this article as: Lagios, E. et al. Testing satellite and ground thermal imaging of low-temperature fumarolic fields: The dormant Nisyros Volcano (Greece). ISPRS Journal of Photogrammetry & Remote Sensing (2007), doi:10.1016/j.isprsjprs.2007.07.003

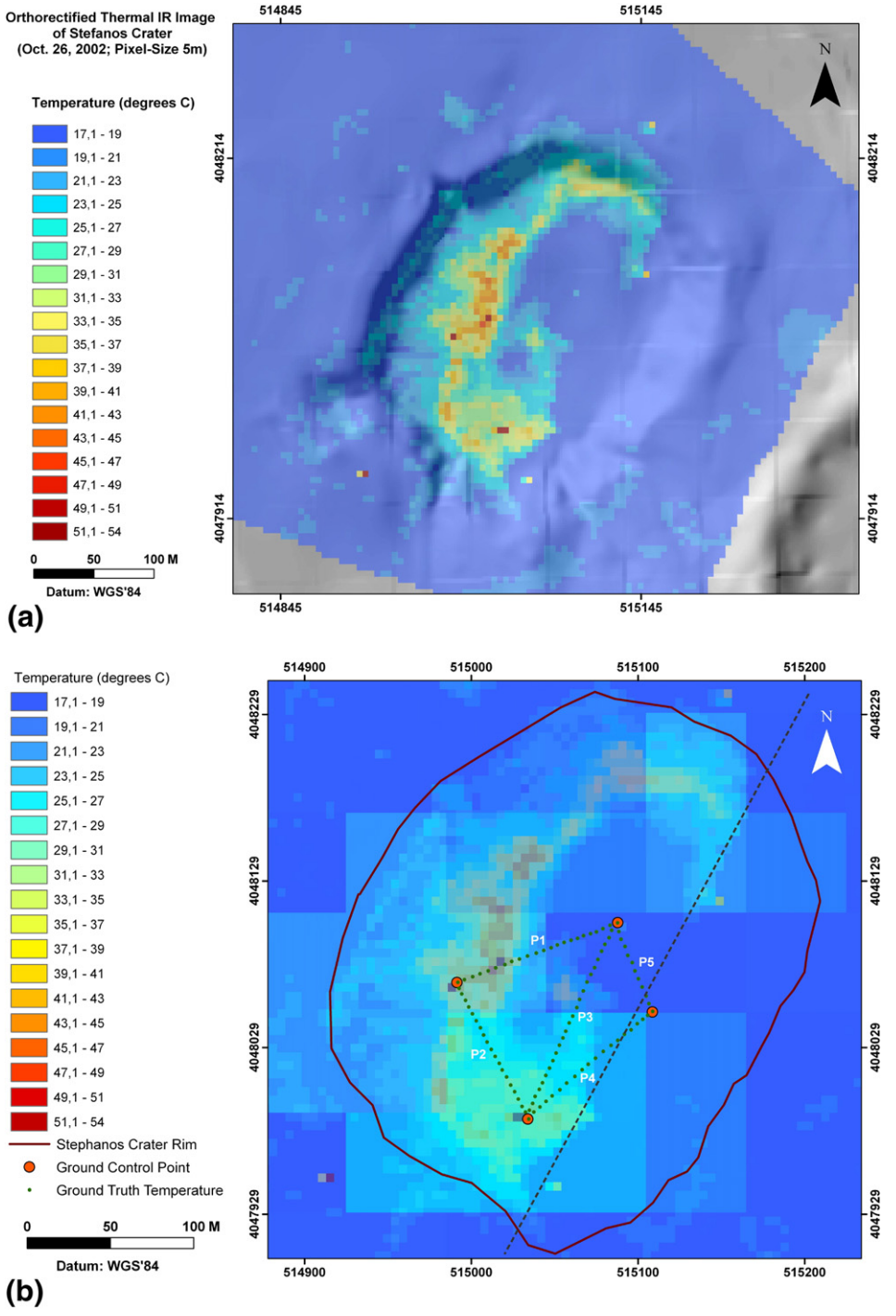

Fig. 7. (a) Orthorectified and calibrated ground TIR image (5 m pixel size) of Fig. 6b, showing temperature variations inside the Stephanos Crater. Note that in the SE part of the crater no data are present due to the low angular view and invisibility from Nikia (SE of dashed line). (b) The orthorectified ground TIR image of Stephanos Crater imposed on the orthorectified Landsat-7 ETM^{+} image together with the legend of the former. Green points along profiles P1 through P5 indicate the ground temperature measurements at 5 m increments.

Please cite this article as: Lagios, E. et al. Testing satellite and ground thermal imaging of low-temperature fumarolic fields: The dormant Nisyros Volcano (Greece). ISPRS Journal of Photogrammetry & Remote Sensing (2007), doi:10.1016/j.isprsjprs.2007.07.003

Fig. 7b superimposes the surface temperatures of the ground TIR image (Fig. 7a) on the satellite TIR image of the same period. The different pixel size of the two types of images can easily be distinguished. A graphical representation of the temperature variation depicted by the ground TIR image and ground temperature measurements (5 m interval) along the five profiles is shown in Fig. 8.

A temperature difference between 0–1 °C was generally observed between the ground temperature measurements and the ground TIR image, while a 2–4 °C difference was noticed along parts of profiles P2 and P3. This is considered satisfactory and, thus, justifies the adopted emissivity values. In profiles P4 and P5, meaningful measurements from the thermal camera should be limited to only 38 m and 31 m, respectively. The rest of these profiles was in the shadow of the crater's rim due to the acquisition angle (15° from the horizon) of the thermal camera. The P1, P2 and P3 profiles cover the western part of the crater's floor which is warmer than the eastern part as it appeared in the Landsat-7 image, as well as in the field measurements.

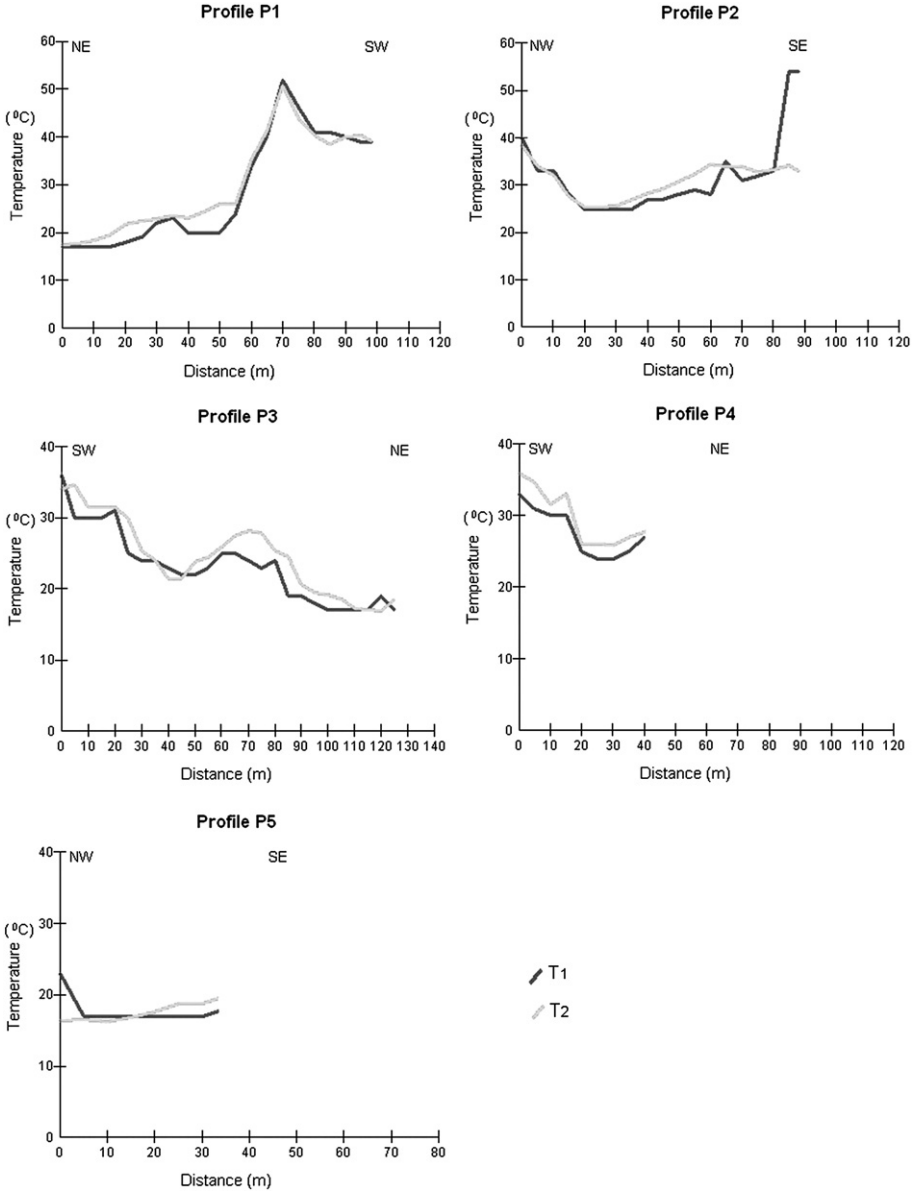

Fig. 8. Temperature variation of ground TIR image (T1) and ground temperature measurements (T2) along the five profiles inside the Stephanos Crater.

Please cite this article as: Lagios, E. et al. Testing satellite and ground thermal imaging of low-temperature fumarolic fields: The dormant Nisyros Volcano (Greece). ISPRS Journal of Photogrammetry & Remote Sensing (2007), doi:10.1016/j.isprsjprs.2007.07.003

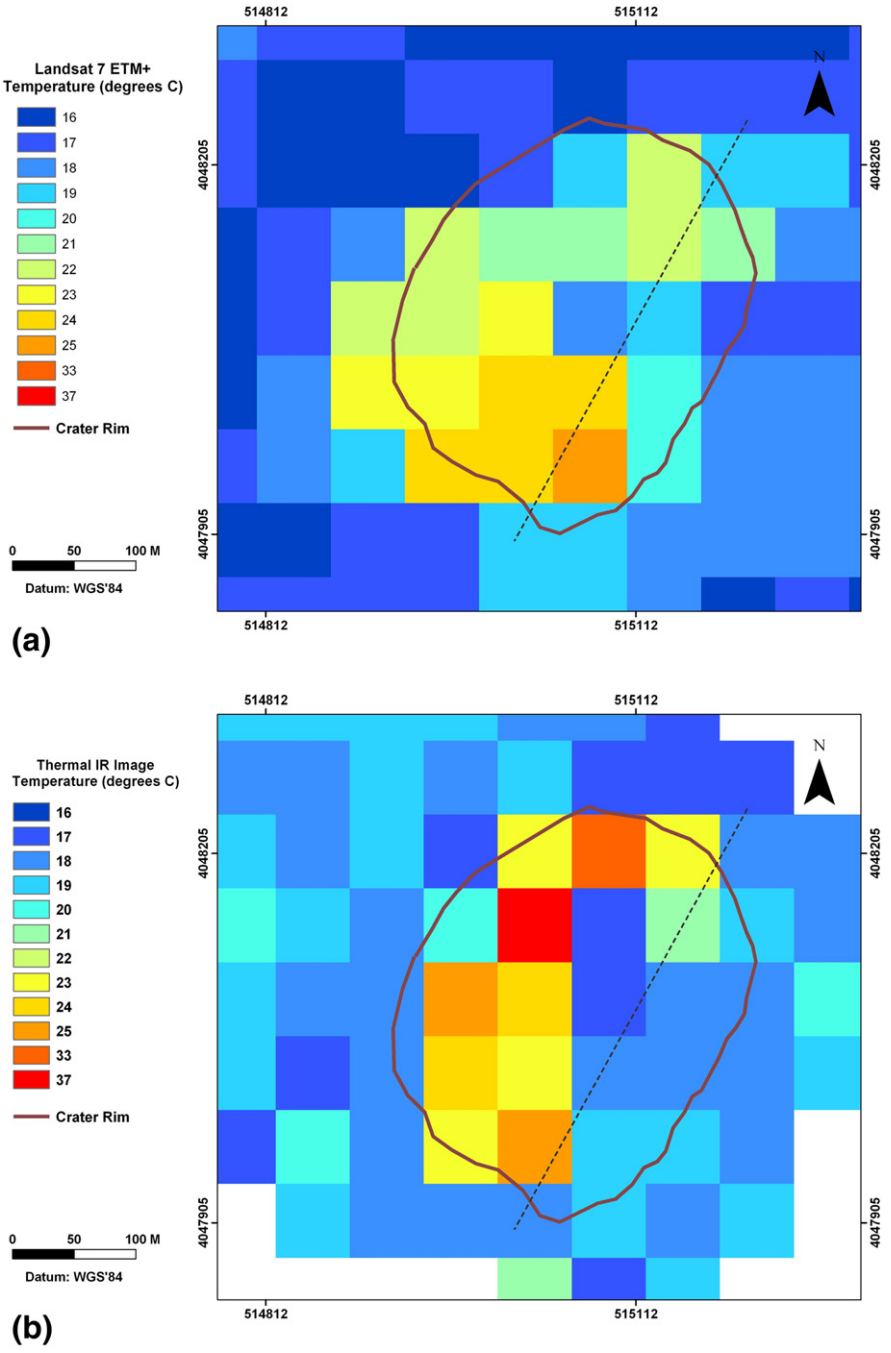

Fig. 9. (a) Landsat ETM$^+$ image of the Stephanos Crater (60 m pixel size) and (b) ground TIR image (5 m pixel size) integrated to a 60 m pixel size for comparison with the Landsat ETM$^+$ image.

Also, many fumaroles occur in this part of the crater, causing large temperature variations over small distances. The high peak observed in P1 at a 75 m distance is due to fumaroles.

The 5 m pixel size of the orthorectified ground TIR image were integrated to 60 m to be compared with the ETM$^+$ image for the part of the Stephanos Crater presented in Fig. 9. This integration was made using the nearest-neighbor resampling method implemented on an ArcGIS platform. The temperature values from the ground TIR camera were generally higher (mean = 23.2 °C) compared to those of the Landsat-7 (mean =

Please cite this article as: Lagios, E. et al. Testing satellite and ground thermal imaging of low-temperature fumarolic fields: The dormant Nisyros Volcano (Greece). ISPRS Journal of Photogrammetry & Remote Sensing (2007), doi:10.1016/j.isprsjprs.2007.07.003

21.6 °C). The high correlation of temperature values between field measurements and the ground TIR image indicates that the camera yields more accurate values than the satellite.

There are 3–4 pixels at the northern edge of the crater, though, which show a relatively higher temperature difference up to about 15 °C (see Fig. 9). The small areal extent of these highly anomalous areas is associated with the occurrence of fine cracks and holes (a few centimeters in dimensions), emitting surface temperatures of 80–90 °C (measured precisely with the thermocouple). These areas are depicted more accurately by the ground camera. The ground TIR images with pixel size of 5 m show temperatures of 32–38 °C, while the pixels after being combined to a larger size of 60 m yield an average of 37 °C. Moreover, the fumaroles, fine cracks and minor holes located on the incline footwall of the rim of the Stephanos Crater are exposed almost perpendicular to the imaging area of the ground TIR camera, revealing much higher temperatures than on the satellite image. Overall for the crater, it is concluded that the resulting temperature difference at most of the pixels is ± 1 °C.

6. Discussion

Thermal remote sensing using band 6 of the Landsat-7 ETM^+ may be regarded as a reliable monitoring tool of low-temperature fumarolic fields of dormant volcanoes. In the case of Nisyros, thermal anomalies with surface temperatures 5–10 °C warmer than their surroundings have been detected inside the caldera. The main anomaly is centred inside the Stephanos Crater, where higher heat fluxes have also been recorded during ground-based geochemical campaigns (Brombach et al., 2003).

Discrepancies between observed and modelled temperatures are due to several factors such as the smoothing of the coarser Landsat image relative to the "point-size" ground observations. From the field data, variations in temperature of about 9 °C were observed at distances of less than 5 m inside the Stephanos Crater. Thus, ground measurement points located on the same pixel of the satellite image may vary by more than 2 °C. In terms of processing, the discrepancies are attributed to differences between the assumed and real land surface emissivity, as well as the applied atmospheric model with the real atmospheric conditions. Moreover, the gases emitted from the fumaroles may not rapidly disperse into the atmosphere, but probably remain for some time inside the caldera or within the atmospheric column above the crater. These unknown factors prevent an accurate determination of the land surface temperature by the satellite sensor. The land surface emissivity was set to a constant value (0.98) for all satellite images. This value is probably not representative of the entire study area, especially within the Stephanos Crater. There are inherent limitations in the processing software such that only a limited number of standard atmospheric models are available and user-defined values cannot be incorporated.

The land surface temperature was essentially constant for the entire island with the exception of the area inside the Stephanos Crater. Here, the temperature increased during the period 2000–2002 by about 4± 2 °C (see Fig. 5). A possible explanation could be an increase in temperature of the hydrothermal system from 230 °C to about 315 °C on the basis of geochemical studies since about 1990 (Chiodini et al., 2002). Higher heat flux and geochemical changes have been observed in the composition of fumaroles as increases of H_2, CO and $^3He/^4He$ ratio (Brombach et al., 2003; Shimizu et al., 2005) after the seismic crisis during 1995–1998 (Lagios et al., 2005).

A portable digital ground TIR camera was employed in our ground study for the first time during 2002. Its use improved the accuracy in measuring the surface temperature of the Nisyros Volcano. If only satellite data are used, the results differ by several degrees Celsius from the observed ground data in some areas of the Stephanos Crater. This discrepancy is due to the irregular distribution of a series of fumaroles aligned along fractures, fine cracks and holes several centimeters across that emit temperatures of up to 90 °C, as well as the distribution of mud pools emitting gases with temperatures exceeding 100 °C.

The use of the ground TIR camera overcame the incapacity of the Landsat satellite to detect hot spots distributed across the island. The camera easily detected from a relatively far distance at least nine thermal springs with temperatures between 30–60 °C. Better results with a higher resolution may be attained in the future and can be an additional low-cost operating feature to aid in monitoring the volcano. The camera is a highly versatile instrument for field calibration in volcanic fields that are difficult to reach. Images may be acquired at any desired time, thus overcoming the time limitation of a satellite overpass. In addition, inaccessible vertical slopes of a crater's rims can be easily monitored. For these reasons, ground TIR cameras are used for on-line, continuous monitoring of the low enthalpy fumaroles of the Vesuvius Volcano (G. Chiodini [Vesuvius Observatory], personal communication).

The Nisyros Volcano is characterized as a low enthalpy field that has the potential to reactivate. Until now, volcanic monitoring could be done only with in-situ observations, i.e. using local seismic and geodetic networks, as well as geochemical measurements. In this

Please cite this article as: Lagios, E. et al. Testing satellite and ground thermal imaging of low-temperature fumarolic fields: The dormant Nisyros Volcano (Greece). ISPRS Journal of Photogrammetry & Remote Sensing (2007), doi:10.1016/j.isprsjprs.2007.07.003

study, a low-cost monitoring system based on satellite and ground thermal imaging was established to form an early warning system. Should an increase of 2–4 °C in surface temperature occur in the future, it will trigger more careful inspection of the low enthalpy field that has now being calibrated to its baseline temperature values.

Acknowledgements

This work was funded by GEOWARN (IST-1999-12310) EU project (www.geowarn.org) and KAPODISTRIAS of the Special Account for Research Grants of the National and Kapodistrian University of Athens. We thank Prof. A. Georgopoulos (NTU, Athens) and Dr. G. Stavrakakis (GI, NOA, Athens) for their help, and the anonymous reviewers for their constructive comments.

References

ATCOR, 2002. ATCOR for ERDAS Imagine. User Manual — Atmospheric and Topographic Correction ATCOR2 and ATCOR3, ed. GEOSYSTEMS, Germany.

Becker, F., Li, Z.L., 1995. Surface temperature and emissivity at different scales: definition measurement and related problems. Remote Sensing Reviews 12 (3–4), 225–253.

Brombach, T., Caliro, S., Chiodini, G., Fiebig, J., Hunziker, J.C., Raco, B., 2003. Geochemical evidence for mixing of magmatic fluids with seawater, Nisyros hydrothermal system, Greece. Bulletin of Volcanology 65 (7), 505–516.

Chen, W., Zhou, G., 2004. Comparison of satellite measured temperatures using Terra, ASTER and Landsat ETM$^+$ Data. Proc. International Geoscience and Remote Sensing Symposium, (IGARSS'04) 3, Anchorage, 20–24 September, pp. 1723–1726.

Chiodini, G., Brombach, T., Caliro, S., Cardellini, C., Marini, L., Dietrich, V., 2002. Geochemical indicators of possible ongoing volcanic unrest at Nisyros Island (Greece). Geophysical Research Letters 29 (16), 1759.

Dash, P., Gottsche, F.M., Olesen, F.S., Fischer, H., 2002. Land surface temperature and emissivity estimation from passive sensor data: theory and practice-current trends (Review article). International Journal of Remote Sensing 23 (13), 2563–2594.

Dawes, G.J.K., Lagios, E., 1991. A Magnetotelluric Survey of the Nisyros Geothermal Field (Greece). Geothermics 20 (4), 225–235.

Dozier, J., 1984. Snow reflectance from Landsat-4 Thematic Mapper. IEEE Transactions on Geoscience and Remote Sensing 22 (3), 323–328.

ESRI, 2001. ArcDoc for ArcGIS, version 8 & 9. http://www.esri.com/ (last accessed June 22, 2007).

Ganas, A., Lagios, E., 2003. Landsat 7 thermal imaging of the Nisyros Volcano. International Journal of Remote Sensing 24 (7), 1579–1586.

Gaonac'h, H., Vandemeulebrouck, J., Stix, J., Halbwachs, M., 1994. Thermal infrared satellite measurements of volcanic activity at Stromboli and Vulcano. Journal of Geophysical Research 99 (B5), 9477–9485.

Geomatica OrthoEngine Basics, 2001. User's Guide version 8.2, ed. PCI Geomatics, (Ontario, Canada).

Geotermica Italiana, 1983. Nisyros 1 geothermal well. PPC-EEC Report, pp. 78–106.

Geotermica Italiana, 1984. Nisyros 2 geothermal well. PPC-EEC Report, pp. 8–44.

GEOWARN, 2003. Final Report of EU Geowarn Project - IST 1999–12310: Geo-spatial warning system, Nisyros volcano (Greece): An emergency case study. (www.geowarn.org).

Gorceix, M.H., 1873a. Sur d' état du volcan de Nisyros au mois de mars 1873. Centre de Recherche Academie de Paris, vol. LXXVII (X), pp. 597–601.

Gorceix, M.H., 1873b. Sur la récente éruption de Nisyros. Centre de Recherche Academie de Paris, vol. 77 LXXVII (XI), p. 1039.

Gorceix, M.H., 1873c. Sur l' éruption boueuse de Nisyros. Centre de Recherche Academie de Paris, vol. LXXVII (XII), pp. 1474–1477.

Gorceix, M.H., 1874a. Phénomènes volcaniques de Nisyros. Centre de Recherche Academie de Paris, vol. LXXVIII (X), pp. 444–446.

Gorceix, M.H., 1874b. Sur l'étude des fumerolles de Nisyros et de quelques-uns des produits de l'éruption de 1873. Centre de Recherche Academie de Paris, vol. LXXVIII(XII), pp. 1309–1311.

Higgins, J., Harris, A., 1997. VAST: a program to locate and analyze volcanic thermal anomalies automatically from remotely sensed data. Computers & Geosciences 23 (6), 627–645.

IRIS, 2001. Temperature Correction of Thermal Imaging Software version 5.6. http://www.infostar.de/iris (last accessed June 25, 2004).

Lagios, E., Sakkas, V., Parcharidis, Is., Dietrich, V., 2005. Ground deformation of Nisyros Volcano (Greece) for the period 1995–2002: results from DInSAR and DGPS observations. Bulletin of Volcanology 68 (2), 201–214.

Marini, L., Principe, C., Chiodini, G., Cioni, R., Fytikas, M., Marinelli, G., 1993. Hydrothermal eruptions of Nisyros (Dodecanese, Greece). Past events and present hazard. Journal of Volcanology and Geothermal Research 56 (1), 71–95.

Oppenheimer, C., 1991. Lava flow cooling estimated from Landsat thematic Mapper infrared data: the Lonquimay eruption (Chile, 1989). Journal of Geophysical Research 96 (13), 21865–21878.

Painter, T.H., Dozier, J., Roberts, D.A., Davis, R.E., Green, R.O., 2003. Retrieval of subpixel snow-covered area and grain size from imaging spectrometer data. Remote Sensing of Environment 85 (1), 64–77.

Papadopoulos, G.A., Sachpazi, M., Panopoulou, G., Stavrakakis, G., 1998. The volcano-seismic crisis of 1996–97 in Nisyros, SE Aegean Sea, Greece. Terra Nova 10 (3), 151–154.

Patrick, M., Dean, K., Dehn, J., 2004. Active mud volcanism observed with Landsat 7 ETM$^+$. Journal of Volcanology and Geothermal Research 131 (3–4), 307–320.

Rothery, D.A., Francis, P.W., Wood, C.A., 1988. Volcano monitoring using short wavelength infrared data from satellites. Journal of Geophysical Research 93 (B7), 7993–8008.

Salisbury, J.W., D' Aria, D.M., 1992. Emissivity of terrestrial materials in the 8–14 μm atmospheric window. Remote Sensing of Environment 42 (2), 83–106.

Schädlich, S., Gottsche, F.M., Olesen, F.S., 2001. Influence of land parameters and atmosphere on Meteosat brightness temperatures and generation of land surface temperature maps by temporally and spatially interpolating atmospheric correction. Remote Sensing of Environment 75 (1), 39–46.

Shimizu, A., Sumino, H., Nagao, K., Notsu, K., Mitropoulos, P., 2005. Variation in noble gas isotopic composition of gas samples from the Aegean arc, Greece. Journal of Volcanology and Geothermal Research 140 (4), 321–339.

Todesco, M., Chiodini, G., Macedonio, G., 2003. Monitoring and modelling hydrothermal fluid emission at La Solfatara (Phlegrean Fields, Italy). An interdisciplinary approach to the study of diffuse

Please cite this article as: Lagios, E. et al. Testing satellite and ground thermal imaging of low-temperature fumarolic fields: The dormant Nisyros Volcano (Greece). ISPRS Journal of Photogrammetry & Remote Sensing (2007), doi:10.1016/j.isprsjprs.2007.07.003

degassing. Journal of Volcanology and Geothermal Research 125 (1–2), 57–79.

Vanderkluysen, L., Volentik, A.C.M, Principe, C., Hunziker, J.C., Hernandez, J., 2005. Nisyros' volcanic evolution: the growth of a strato-volcano. In: Hunziker, J.C., Marini, L. (Eds.), The Geology Geochemistry and Evolution of Nisyros Volcano (Greece) Implications for the Volcanic Hazards. Mémoires de Géologie (Lausanne), vol. 44, pp. 100–106.

Vassilopoulou, S., Hurni, L., 2001. The use of digital elevation models in emergency and socio-economic planning: a case study at Kos-Yali-Nisyros-Tilos islands, Greece. Proc. 20th International Cartographic Conference, Beijing, China, 6–10 August 2001, pp. 3424–3431 (on CDROM).

Vassilopoulou, S., Hurni, L., Dietrich, V., Baltsavias, M., Pateraki, M., Lagios, E., Parcharidis, I., 2002. Ortho-photo generation using IKONOS-2 imagery and high resolution DEM: a case study on monitoring the Volcanic Hazard on Nisyros Island (Greece). Journal of Photogrammetry and Remote Sensing 57 (1–2), 24–38.

Volentik, C.M., Vanderkluysen, L., Principe, C., Hunziker, J.C., 2005. Stratigraphy of Nisyros Volcano. In: Hunziker, J.C., Marini, L. (Eds.), The Geology Geochemistry and Evolution of Nisyros Volcano (Greece) Implications for the Volcanic Hazards. Mémoires de Géologie (Lausanne), vol. 44, pp. 26–66.

Wan, Z., Ng, D., Dozier, J., 1994. Spectral emissivity measurements of land-surface materials and related radiative transfer simulations. Advances in Space Research 14 (3), 91–94.

Please cite this article as: Lagios, E. et al. Testing satellite and ground thermal imaging of low-temperature fumarolic fields: The dormant Nisyros Volcano (Greece). ISPRS Journal of Photogrammetry & Remote Sensing (2007), doi:10.1016/j.isprsjprs.2007.07.003